Dynamics of bubble breakup under turbulent flow conditions

Downloaded from: https://research.chalmers.se, 2025-04-24 15:02 UTC

Citation for the original published paper (version of record):
Vikash, V., Andersson, R. (2025). Dynamics of bubble breakup under turbulent flow conditions. Chemical Engineering Journal, 511. http://dx.doi.org/10.1016/j.cej.2025.162019

N.B. When citing this work, cite the original published paper.

research.chalmers.se offers the possibility of retrieving research publications produced at Chalmers University of Technology. It covers all kind of research output: articles, dissertations, conference papers, reports etc. since 2004. research.chalmers.se is administrated and maintained by Chalmers Library

(article starts on next page)

Chemical Engineering Journal 511 (2025) 162019

Contents lists available at ScienceDirect

Chemical Engineering Journal

journal homepage: www.elsevier.com/locate/cej

Dynamics of bubble breakup under turbulent flow conditions☆

Vikash Vashisth, Ronnie Andersson *

Department of Chemistry and Chemical Engineering, Chalmers University of Technology, SE-41296 Gothenburg, Sweden

ARTICLE INFO

Keywords:
Turbulence
Bubble
Breakup
Internal flow
Multiphase flow

ABSTRACT

This study provides unique insights into the dynamics of bubble deformation and breakup under turbulent flow conditions, utilizing both experimental measurements and high-resolution simulations and unveils information that has been previously unattainable with current methods. The simulations are rigorously validated against experimental data obtained under identical hydrodynamic conditions, and enable analyzes of the interfacial dynamics, breakup time scales, daughter size distributions, and internal flow mechanisms, crucial for advancing future model development. Overall, the dynamic deformation and statistical data show very strong agreement with experimental measurements and reveal an inherent stochastic behavior of bubble breakup due to turbulent interactions. For the first time, details of the internal flow mechanism during bubble breakup have been resolved, revealing development of flow velocities up to 30 times greater at the bubble neck compared to the mean bubble velocity. Analysis reveals that the characteristic internal redistribution flow occurs within a fraction of a millisecond, necessitating a temporal resolution of 20,000 frames per second. The development of an accelerating internal flow is quantified throughout the process until a sudden termination of the flow occurs due to the rapidly shifting balance of stresses at the interface. This ultimately leads to the breakup and formation of unequal sized daughter fragments, approximating a U-shaped distribution, with consistent results in both experimental and simulation data. Evidence suggests that bubble breakup at higher Weber number can form satellite fragments like what is known from droplet breakup, but these are likely beyond the resolution capabilities of the most advanced experimental setups documented in single bubble breakup literature. Consequently, simulations offer a more comprehensive understanding of bubble dynamics, surpassing current experimental capabilities due to their superior temporal and spatial resolutions and the absence of complications from light reflection and refraction at interfaces. The details and quantifications presented in this study are anticipated to contribute significantly to the development of refined breakup kernels.

1. Introduction

Breakup of fluid particles is a common phenomenon in most multiphase systems, and mastering the control of particle breakup, as well as their size distribution in turbulent multiphase flows, offer numerous advantages. These include enhanced mass and heat transfer, improved product quality, optimized chemical reactors, increased process efficiency, and more effective predictive modeling and control. Despite significant efforts to unveil these complex phenomena a better understanding of bubble dynamics and breakup is still required to establish reliable models. Theoretical advancements have been made over several decades, beginning with the pioneering work of Kolmogorov [1] and Hinze [2]. However, the intrinsic complexity of these phenomena, characterized by interactions with turbulent vortices occurring on millisecond time scales and exhibiting intricate three-dimensional motion, makes experimental analysis exceptionally challenging.

Over the years, experiments have been conducted to study the breakup of fluid particles within various devices [3–12]. However, there remains a scarcity of experimental data and high-speed imaging within the turbulent flow regime for single fluid particle breakup, limiting comprehensive validation of the breakup models. To the best of the authors knowledge, measurements up to a maximum of 4000 frames per second (fps) have been successfully demonstrated in the literature, which is insufficient to resolve the dynamics of the internal flow during bubble breakup. Additionally, high-speed imaging faces inherent limitations and trade-offs; as frame rates increase, resolution diminishes due to the reliance on partial readout of CCD camera chips. Furthermore, laser-based techniques are inadequate for measuring the flow field

☆ This article is part of a special issue entitled: 'ISCRE 28' published in Chemical Engineering Journal.

* Corresponding author at: Department of Chemistry and Chemical Engineering, Kemivägen 4, Chalmers University of Technology, SE-41296 Gothenburg, Sweden.
E-mail address: ronnie.andersson@chalmers.se (R. Andersson).

https://doi.org/10.1016/j.cej.2025.162019

Available online 26 March 2025
1385-8947/© 2025 The Authors. Published by Elsevier B.V. This is an open access article under the CC BY license (http://creativecommons.org/licenses/by/4.0/).

inside and around bubbles due to reflection and refraction occurring at interfaces, stemming from the inability to achieve index matching between the gas and liquid phases. Despite achievements in experimental systems aimed at resolving bubble dynamics and breakup, a clear lack of data and understanding persists, as noted by researchers in the field. Recently, Ni [13] reviewed the deformation and breakup of fluid particles in turbulence. Consequently, these experimental challenges are likely to persist in the foreseeable future, hindering comprehensive validation of theoretical models.

Modeling the breakup process in multiphase systems requires the coupling of computational fluid dynamics (CFD) and population balance modeling (PBM) [14–16]. The CFD-PBM coupled model quantitatively estimates the breakup process, and for reliable predictions, the breakup kernel is found to be a crucial for achieving better accuracy [17,18]. Over the years, various statistical and theoretical breakup models, along with different assumptions used in developing such models, have been reviewed by several authors, including Lasheras et al. [19], Liao and Lucas [20], Solsvik et al. [21], and Foroushan and Jakobsen [22]. Models for fluid particle breakup have been developed based on the interactions between fluid particles and turbulent vortices and are ideally validated using experimental data on single fluid particle breakup, breakup rate and size distribution [23–32]. Breakup occurs when disruptive external fluid dynamic stresses exceed cohesive stresses, which act to restore the fluid particle to its lowest energy state i.e. spherical shape. Under the influence of disruptive stress, the bubble deforms mainly due to the normal stress from turbulence, forming a neck or thread depending on the fluid properties, before ultimately breaking into two or more fragments. To overcome the limitations of experimental systems, highly resolved simulations such as Large Eddy Simulation (LES) and Direct Numerical Simulation (DNS) can be employed, albeit at significant computational expense. These advanced simulations can provide intricate details about the physics inside and around fluid particles, allowing for exceptionally high spatial and temporal resolution. By capturing the complex interactions and dynamics that occur during the breakup process, DNS and LES can yield valuable insights that are otherwise inaccessible through experimental methods alone. These simulations can account for the stochastic nature of turbulence, accurately modeling the energy transfer from vortices, and the subsequent deformation and fragmentation of fluid particles. Moreover, the ability of DNS and LES to simulate a wide range of flow conditions and fluid properties further enhances their utility in validating theoretical models. The detailed information derived from these simulations can bridge the gap left by experimental constraints, offering a robust framework for understanding and predicting the behavior of fluid particles in turbulent multiphase flows.

Recent advancements have shown that the fluid particles breakup can be effectively simulated using three-dimensional transient simulations [33–39].

Despite the high computational costs, the advantages of high-resolution simulations in advancing our understanding and enhancing predictive modeling capabilities are well-documented in literature. Significant progress has been made in using advanced simulations to study the breakup of liquid droplets in turbulent flow conditions. However, numerical simulation methods for the breakup of gas bubbles remain to be developed and used to enhance our understanding of the unique underlying phenomena associated with gas bubbles, which differ significantly from those of liquid droplets [28]. While the initial breakup stages are similar for both bubbles and drops, bubbles tend to break into fragments of unequal size due to apparent internal flow redistribution. Wang et al. [30,31] adopted this concept and proposed models that accounts for the mechanism of internal flow. While their model incorporates several assumptions to bridge existing gaps, such as limiting breakup to binary fragmentation, laminar flow conditions within the bubble neck, and maintaining a constant ratio between the neck diameter and the radius of the smaller side of the deformed bubble, it represents a significant advancement toward the development of reliable breakup kernels.

Therefore, high-resolution simulations are considered the most suitable approach for achieving the goal of necessary spatial and temporal resolution to capture the dynamics of bubble breakup under turbulent flow conditions. This work aims to develop a simulation methodology that enables detailed investigation of bubble dynamics and gain deeper understanding of the underlying breakup phenomena. The key contributions of this study include the development of methodology and rigorous validation of single air bubble breakup against experimental data obtained under identical hydrodynamic conditions. These efforts are intended to build confidence in the simulation results and provide conclusive insights into the dynamics that were previously speculative due to inadequate means for studying and quantifying the phenomena.

2. Experimental methodology

The experimental setup comprises a flow reactor and a high-speed imaging system used to analyze bubble behavior under turbulent flow conditions. The reactor is equipped with transparent, non-curved walls, providing an ideal setup for using an intense light source without image distortion. The reactor is equipped with multiple small mixing elements to ensure the continuous generation of turbulence. The experimental setup is illustrated in Fig. 1 and more details about the reactor are available in the literature by Andersson and Andersson [28] which highlights the systems capability to provide favorable conditions, including a well-defined main flow direction, low linear velocity, and relatively high turbulence compared to other systems used for breakup studies. Particle image velocimetry (PIV) measurements of the same experimental system have also confirmed the more homogeneous turbulent properties of the reactor [40].

The camera's recording rate was set at 4000 frames per second, with a short exposure time of 10 μs for obtaining sharp images. A hybrid lighting system was employed to capture sharp images, with an image resolution of 309,000 pixels/cm2 and 8-bit depth, allowing the measurement of all fragments down to 50 μm upon breakup. A low holdup of the dispersed phase (single bubble) was maintained to avoid coalescence and turbulence modulation during the experiments. Air and deionized water were used as the dispersed and continuous phases, respectively. The physical properties of the fluids at room temperature are provided in Table 1.

Bubbles of varying sizes were generated using nozzles with different diameters, creating distinct size bins for the experiments. The experiments were conducted under a range of flow conditions, as detailed in Table 2. All measurements were performed at a constant temperature of 20 °C, with thermocouple measurements ensuring an accuracy of ± 0.1 °C. Additionally, a flow rate error margin of less than 1 % was maintained to ensure experimental precision. The uncertainties in fluid density and viscosity were 0.03 % and 0.2 %, respectively. Table 2 also provides the Taylor scale Reynolds number, $Re_\lambda = u'\lambda/\nu$, which quantifies the inertial forces relative to the viscous forces at the Taylor microscale, λ, an intermediate scale in turbulent flows between the smallest dissipative scales (Kolmogorov scales) and the larger energy-containing scales. This metric offers additional insights beyond the traditional bulk Reynolds number regarding existence of inertial subrange. Consequently, this data shows that the study is conducted under conditions relevant to many chemical engineering systems, specifically at a level where an inertial subrange exists.

3. Simulation methodology

3.1. Governing equations

In this study, high-resolution simulations using the multiphase volume of fluid method coupled with large eddy simulations of turbulent flow are developed to investigate the dynamics of bubble deformation

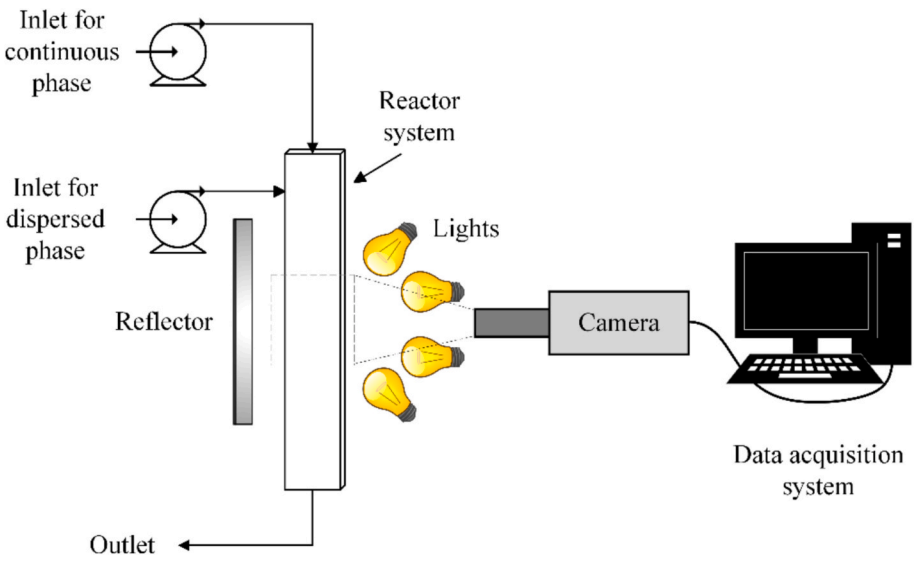

Fig. 1. Configuration of the high-speed imaging system for measuring dynamics of bubble breakup.

Table 1
Fluid properties of the continuous and dispersed phases.

Phase	Density [kg/m^3]	Viscosity [mPas]	Interfacial tension [mN/m]
Water	998.2	1.0	72.0
Air	1.225	0.02	

Table 2
Flow parameters and experimental conditions.

System/Flow rate (l/h)	200	250
Taylor scale Reynolds number	69	77
Turbulent energy dissipation rate, ε [m^2/s^3]	8.54	16.4
k/ε	7.5	6.0

and breakup. The simulation methodology is validated with experimental results obtained under identical geometric and hydrodynamic conditions. At high Reynolds numbers, the computational cost of direct numerical simulation become prohibitively high, as it scales with the cube of Reynolds number [41]. Consequently, this study employs large eddy simulations to resolve the turbulent eddies that interact with the secondary phase, enabling the dynamics of deformation and breakup to be quantified. The effect of smaller isotropic turbulent eddies are modeled using sub-grid scale models [42]. In LES, a filtering operation is applied to decompose the velocity field $u(x,t)$ into a resolved velocity field $\overline{u}(x,t)$ and unresolved velocity field, $u'(x,t)$. The filtered governing Navier-Stokes equations for two-phase incompressible flow are given in Eq. (1) and Eq. (2)

$$\nabla \bullet \overline{u} = 0 \tag{1}$$

and,

$$\rho\left(\frac{\partial \overline{u}}{\partial t} + \overline{u} \bullet \nabla \overline{u}\right) = -\nabla \overline{p} + \rho g + \nabla \bullet \left[\left(\mu + \mu_{sgs}\right)\left(\nabla \overline{u} + \nabla^T \overline{u}\right)\right] + F_i \tag{2}$$

where, g and μ represents the gravitational acceleration and viscosity respectively. Here, p and ρ represent pressure and density, respectively. Additionally, μ_{sgs} and F_i, denote the sub-grid scale turbulent viscosity and interfacial tension force, respectively. These two unknown terms in the momentum equation must be accurately modeled. The dynamic Smagorinsky-Lilly model was used to model the sub-grid turbulent viscosity [43]. F_i acts as a source term in the momentum balance equation due to the local interfacial tension force and was calculated by using the continuum interfacial tension force model proposed by Brackbill et al. [44].

The magnitude of the interfacial tension force, F_i, is determined by both the interfacial tension coefficient, σ, and the local curvature of the interface, κ, as shown in Eq. (3). The direction of the force is defined by the unit normal vector to the interface, n, as defined in Eq. (4).

$$F_i = \sigma \kappa n_i \delta_s \tag{3}$$

The unit normal vector to the interface, n_i, is derived from the gradient of phase fraction, α and is given by

$$n_i = \frac{\nabla \alpha}{|\nabla \alpha|} \tag{4}$$

The curvature is given by

$$\kappa = -\nabla \bullet n_i \tag{5}$$

Therefore, the local source term in the momentum balance is closed by

$$F_i = \sigma \nabla \bullet \left(\frac{\nabla \alpha}{\|\nabla \alpha\|}\right) \bullet \nabla \alpha \tag{6}$$

Furthermore, the transport equation for phase fraction is calculated using Eq. (7).

$$\frac{\partial \alpha}{\partial t} + \overline{u} \bullet \nabla \alpha = 0 \tag{7}$$

The density ρ and dynamic viscosity μ are given by Eqs. 8–9, where the subscripts denote the continuous phase, c, and dispersed phase, d, respectively.

$$\rho = \alpha \rho_c + (1-\alpha)\rho_d \tag{8}$$

$$\mu = \alpha \mu_c + (1-\alpha)\mu_d \tag{9}$$

Simulations were conducted using a dynamic adaptive meshing strategy combined with an interface reconstruction scheme to maintain high resolution around interface. This dynamic adaptive meshing strategy is feasible for balancing computational cost while preserving solution accuracy. The pressure–velocity coupling equation was solved using the SIMPLE method. Spatial discretization of the momentum equation and temporal discretization were done using bounded central differencing and first-order implicit schemes, respectively. To ensure time step in-

dependence for first-order implicit schemes and account for the uncertainty in the outcomes of both breakup and non-breakup scenarios, a small time step size of 2.5 μs was used in simulations. Given that the breakup time scale observed in experiments is a few milliseconds, this offers a significantly higher resolution, approximately 1000 times finer than the breakup event. As such the temporal resolution of simulations, 400 000 fps, provides ample opportunities to characterize the rapid dynamics of bubble breakup.

To accurately capture the interface in the multiphase system a modified high-resolution interface capturing (HRIC) scheme with a strict volume fraction cutoff limit of 10^{-6} was employed. Additionally, dynamic interfacial anti-diffusion was utilized, minimizing numerical diffusion and ensuring a sharp interface during the simulations. A precise cutoff limit was applied for coarsening and refinement in regions with high gradients at the interface, ensuring detailed and accurate simulation results. A dynamic adaptive meshing methodology was used, providing high resolution across the interface, the scale of refinement allowed resolution of $d_0/100$, ensuring that the flow both within the bubble and around its interface, was fully resolved. The governing equations were solved on high-performance computing clusters using Ansys Fluent 2022R2.

The flow reactor was discretized using a high-quality bulk mesh complemented by prism layers at the wall with resolution of $y^+ = 1$, to enable the dynamic subgrid model to accurately resolve the near-wall region. The mesh resolution and time step size were evaluated to ensure the ratio of resolved turbulent kinetic energy is high. 94 % of the turbulent kinetic energy was resolved, significantly exceeding the general recommendation of resolving 80 % [42,45]. A sequential injection of one millimeter single bubbles was applied at random locations in the bulk, thus maintaining very low bubble holdup and preserving the turbulence homogeneity observed in the experiments by using identical operating condition. Data collection commenced after the simulations had run for a time surpassing the characteristic timescale of the largest turbulent vortices. This approach ensured that the results were independent of the initial conditions.

The interaction between bubbles and vortices is inherently random due to the stochastic nature of turbulence. Breakup events occur only when the interaction between the bubbles and vortices is sufficiently strong, meaning that the disruptive stress exceeds the cohesive stress; otherwise, no breakup event takes place. This means that both bubble breakup and non-breakup cases were sampled. A methodology similar to that of Karimi and Andersson [34] was employed to statistically evaluate these cases. By utilizing parallelization on a high-performance computing cluster, feasible computation times were achieved. In total, more than 2 million core hours were required for all breakup and non-breakup cases. Postprocessing of the results allowed for statistical validation of the breakup process, and data analysis were used to unveil intricate details of the bubble dynamics, as elaborated on in the results section.

3.2. Dynamic adaptive mesh methodology

Due to the continuous advection of the dispersed phase interface within the computational domain, dynamic mesh refinement and coarsening is essential. In this study, dynamic remeshing is used to enable simulations of bubble dynamics by employing adaptive refinement and coarsening criteria, with specific cutoff values scaled by global maxima of 0.01 and 0.02, respectively. Fig. 2a-c presents a detailed view of the refined mesh surrounding the interface of the dispersed phase for three distinct moments: the initial mother bubble, a significantly deformed bubble, and a small fragment resulting from the breakup. For each scenario, the mesh is displayed on a cross-sectional plane that intersects the center of the bubble, demonstrating the efficiency of adaptive refinement and coarsening during the dynamic process. Multiple refinement levels were evaluated to identify mesh independence, with the fourth level found to capture independent bubble dynamics and resolving the smallest fragments. As illustrated in Fig. 2c, the high resolution achieved in simulations surpasses that of experimental setups, which are constrained in their ability to accurately resolve fragments smaller than 50 μm. The simulations results discussed in the results section are based on this mesh-independent configuration.

4. Results and discussion

The experimental measurements and high-resolution simulations were conducted under identical hydrodynamic conditions, enabling validation and analysis. Statistical validation includes key parameters such as aspect ratio before breakup, breakup time, and the distribution of daughter bubble sizes. Postprocessing of the results allows detailed analysis and understanding of bubble breakup mechanisms, including energy transfer dynamics, stress distribution, pressure gradients inside the bubbles, the internal flow and subsequently the formation of unequal size fragments. Consequently, these efforts offer conclusive insights into the complex dynamics of bubble behavior at temporal and spatial scales that are unachievable through experimental means alone.

4.1. Validation of bubble deformation and breakup time scale

While the high-resolution simulations provide superior temporal and spatial resolution compared to the state-of-the-art experimental setups presented in the literature, it is crucial to ensure that the predictions are reliable. This validation involves confirming that the disruptive stresses are quantitatively accurate and leads to correct deformation dynamics and breakup time scale. Given the experimental conditions with moderate Weber numbers, not all bubbles break. A continuous interaction of bubbles and turbulent vortices inside the reactor leads to bubble deformation and occasionally breakup. Both experiments and simulations reveal small-scale bubble interface dynamics induced by turbulence, with significant deformation consistently occurring before

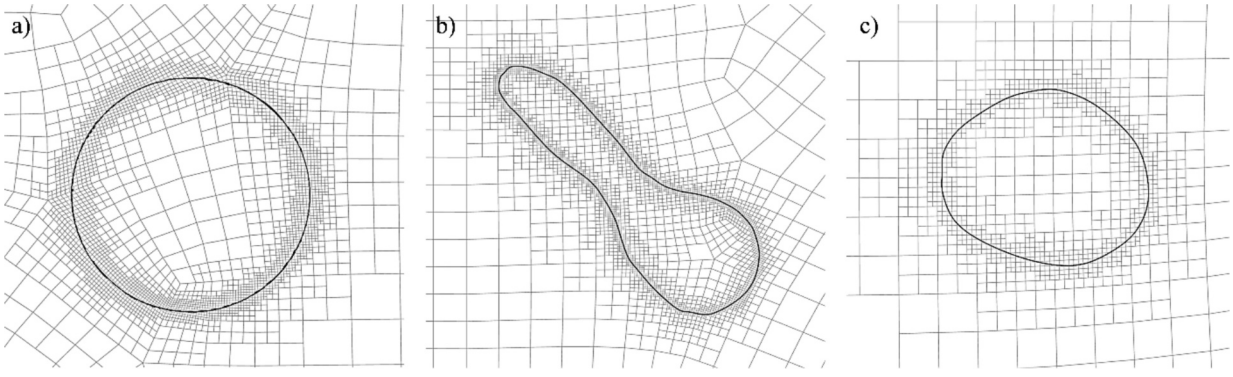

Fig. 2. Cross-sectional views illustrating the dynamic mesh adaption adaptation with different magnifications for clarity: a) initial patching of a 1000 μm mother bubble, b) a highly deformed bubble, and c) an 80 μm fragment. The *iso*-line shows the phase function $\alpha = 0.5$.

breakup. A key measure of this deformation is the aspect ratio, defined as $z = l/d_0$, where l is length of the deformation axis and d_0 is initial bubble diameter. The deformation was measured at different flow rates and categorized into two Weber number classes: 0.3 and 0.5 respectively. Weber number is defined as the ratio of turbulent inertial force, considering a vortex of the same size as the bubble, to the interfacial tension force [8]. Fig. 3 shows that the experimentally and numerically measured bubble deformations are similar. The aspect ratio extends up to 3.5, whereas the peak falls within the range of 2 to 2.5.

The bubble breakup time scale is a crucial variable for evaluating the accuracy of the numerical simulations. Here the breakup time scale is defined as the duration from when a bubble transitions from a predominantly spherical shape to the instance when the fragmentation occurs. This time scale is expected to be bounded by the integral turbulent time scale. Table 3 shows good agreement between experimental measurements and simulations in general. The average breakup time, ranging from 1/2 to 2/3 of the turbulent time scales, indicates its connection to moderate to larger scales of turbulent structures.

According to the available literature, this study is the first to successfully predict and validate bubble breakup with experimental measurements under the same hydrodynamic conditions. This advancement enables an analysis of interfacial energy, which requires information about the three-dimension shape at each moment during the breakup process, a property which is unattainable with experimental data relying on high-speed two-dimensional imaging. By employing surface integration of precise three-dimensional simulations, the interface energy can be quantified with unique precision since the interfacial energy is a function of the interfacial tension coefficient and the instantaneous interfacial area. The normalized interfacial energy (γ) is defined by Eq. (10),

$$\gamma(t) = \frac{\sigma A(t)}{\sigma A_0} = \frac{A(t)}{A_0} \tag{10}$$

where, σ and $A(t)$ are the interfacial tension and the interfacial area, respectively. Here A_0 denotes the minimum energy, i.e. $\gamma = 1$, which corresponds to a spherical bubble shape. Analysis of the normalized interfacial energy, γ, shows that it typically ranges from 1 to 1.1 prior to breakup while it reaches values between 1.3–1.5 at instances just before breakup occurs. The peak value, representing the maximum deformation, occurs immediately before the interface divides into two or more daughter bubbles. Fig. 4 demonstrates that the simulation results for one millimeter bubble at 0.5 Weber number are consistent with the experimental data, showing a specific case of 35 % increase in interfacial

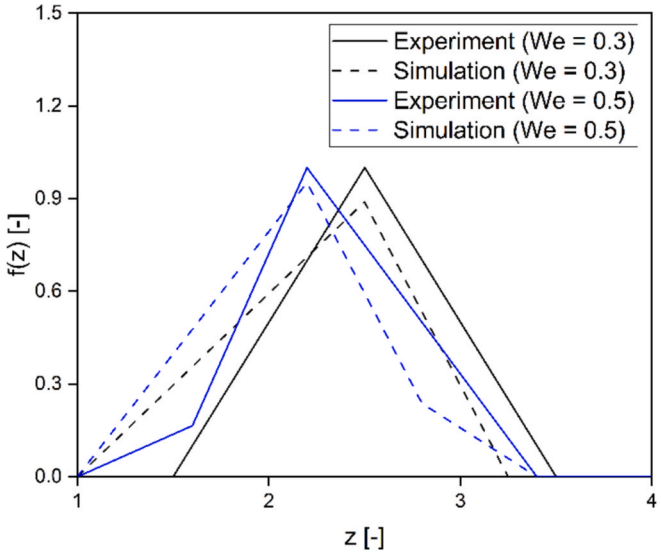

Fig. 3. Deformation prior to bubble breakup at different Weber numbers.

Table 3
Validation of bubble breakup time and relationship to the turbulent time scale.

Scale	Experiment (We = 0.3)	Simulation (We = 0.3)	Experiment (We = 0.5)	Simulation (We = 0.5)
Mean time [ms]	3.8	3.6	3.4	3.4
Variance [ms^2]	1.2	1.1	0.9	0.8
Integral turbulence time scale [ms]	7.5	6.0	7.5	6.0

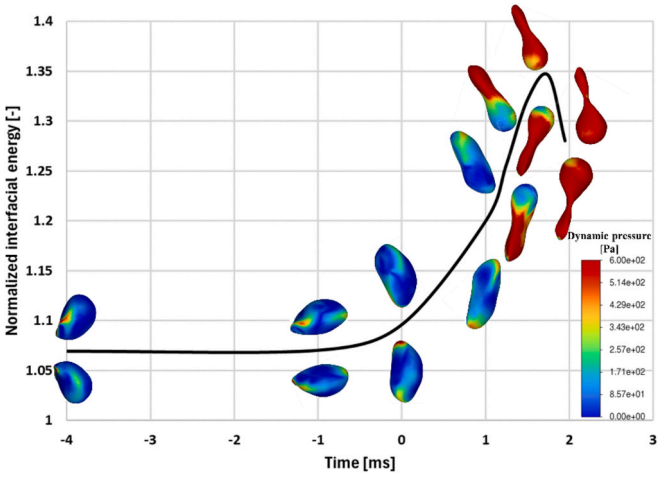

Fig. 4. Normalized interfacial energy superimposed with dynamic pressure distribution, at specific times, t = -4.00, −1.00, 0.00, 1.00, 1.50, 1.75, and 1.95 [ms].

energy. On average, the characteristics of the increase in normalized interfacial energy in simulations are approximately 40 %±10 %. The dynamic pressure distribution, calculated based on the mean bubble motion (center of mass), is superimposed with the normalized interfacial energy in Fig. 4. The bubble images are mirrored along the x-axis to display both front and rear views of the dynamic pressure distribution.

Initially, the dynamic pressure exerted on the bubble interface is low, keeping the bubble mostly spherical (time $\leq$ 0 ms). As the dynamic pressure increases on the interface and surpasses the stabilizing stress, the bubble can no longer maintain its spherical shape. With the increase in dynamic pressure on the interface, the bubble begins to deform due to interaction between turbulent flow field and the bubble. After 1 ms, the dynamic pressure distribution becomes asymmetric between the two ends of the bubble, creating a small but significant pressure difference. Subsequently, the interfacial energy starts to go down before the bubble breaks into daughter fragments. Section 4.2 provides a statistical validation analysis of the resulting daughter size distribution. Meanwhile, section 4.3 provides a comprehensive analysis of the development of self-accelerating internal flows, which leads to daughter fragments of unequal sizes.

4.2. Bubble breakup and daughter size distribution

In the literature on drop and bubble breakup, a common assumption is that binary breakup occurs, and most models address only binary breakup [25,46,47]. However, experimental evidence suggests that droplets are more likely to undergo multiple fragmentation, while bubbles predominantly follow a binary breakup pattern [4,8,28,48]. The successful identification of the total number of fragments formed upon breakup is often limited by camera resolution and the field of view, potentially leading to undetected smaller fragments in experiments. By comparing experiments and simulations conducted under identical hydrodynamic conditions, the capability of simulations in capturing the smallest bubble fragments becomes evident. The experimental setup,

constrained by a camera resolution limit of 50 μm, prevents identification of fragments smaller than the resolution threshold. In contrast, high-resolution simulations, which use mesh refinement without a lower size limit, occasionally reveal formation of satellite fragments as small as 10 μm, which remain undetectable by current experimental systems and standards. Thus, simulations provide more precise quantification due to better spatial resolution. Fig. 5 compares experimental and simulation results for a 1 mm diameter mother bubble. The experiment, recorded at 4000 fps, showed continuous deformation leading to breakup after approximately 2 ms, producing two fragments. The largest fragment contained 95 % of the total volume, and the smaller 5 %, consistent with previous studies indicating unequal-sized bubble breakup in turbulent flows [28].

Notably, the simulation displayed a similar initial deformation pattern and breakup time as the experiment, but also revealed the formation of small satellite fragments that were below the detection limit of the experimental setup, as seen in the zoomed-in magnification at the last time frame. To improve future modeling efforts, the prevailing assumption of binary fragmentation in bubble breakup can be reconsidered, as smaller fragments, with their higher surface-area-to-volume ratio, can affect interfacial mass transfer and should be accounted for in more sophisticated models.

Fig. 6 illustrates the stochastic nature of bubble breakup in turbulent flows by presenting two experimental observations side by side. In both cases, the bulk hydrodynamic conditions and the initial size of the mother bubble are identical. However, the breakup dynamics differ significantly, due to encounters with different turbulent structures. This means that bubbles don't interact with the mean turbulence, instead there will be new turbulent vortices surrounding which will control the outcome, since the time scale of the breakup and lifetime of vortices have the same order of magnitude. This emphasizes the need for simulations to better understand the interaction. In Fig. 6a, rapid deformation occurs up to 1.00 ms, followed by a relaxation period before the breakup event. Conversely, Fig. 6b shows a more gradual deformation until 1.75 ms, after which a sudden breakup into distinct fragments occurs. These differences in dynamics lead to varying final outcomes. For the two examples shown, the volume fraction of the largest fragment is 98 % in Fig. 6a, whereas it is 84 % in Fig. 6b. This demonstrates how slight variations in the breakup process can result in markedly different fragment distributions, and requires statistical validation as presented by the end of this section.

In comparison, the high-resolution simulations display remarkable similarities in dynamics and by collecting different realizations of the stochastic process, as illustrated by Fig. 7, and further supported by validation of breakup time scale and daughter size distribution.

Despite both experiments and simulations reveal similar trends with unequal volume fractions, simulation offer the capability of identifying satellite fragments as small as 25 μm, a size clearly below the detection threshold of the experimental system. These small satellites might be attributed to the high internal flow velocities that develop and low inertia of the gas phase (as discussed in the next section). This further reinforces the complexity of the breakup process in turbulent flows, where small variations in flow dynamics can lead to significantly different fragmentation outcomes. A statistical analysis shows that the likelihood of producing un-equal sized fragments is significantly higher than generating equal-sized fragments. As shown in Fig. 8, the daughter size distribution adheres to a U-shaped pattern within the examined range of Weber number. Here f_{bv} refers to the volume ratio of the largest fragment to the mother bubble. This pronounced tendency towards unequal sized fragmentation is primarily due to the inherent internal bubble hydrodynamics, which is examined in greater detail in the subsequent section through an exploration of the stresses and internal flow field that develops during the breakup process.

The agreement in interfacial dynamics observed from 2D images during breakup and quantification of breakup time scale, accurately determined from 2D data as the neck rupture is clearly visible, implies that the internal flow is correct and shows that the rupture is predicted correctly. The internal flow field is further supported by statistical validation of daughter size distribution, where quantification based on 2D images is accurate since smaller daughters tend to have a more spherical shape. Overall, these factors all imply that the flow field and stresses during bubble deformation and breakup are predicted accurately.

4.3. Internal flow mechanism

By utilizing the significantly higher temporal and spatial resolution in simulations, the mechanisms responsible for the formation of unequal-sized daughter fragments can be visualized and analyzed at the level of individual bubbles. This section analyzes the internal flow mechanism and emphasizes the role of stresses during the critical stages of bubble breakup. In a high-turbulent flow field, the bubble remains in constant motion and does not reach a state of complete relaxation. The bubble undergoes minor deformations from its spherical shape, due to the surrounding turbulent flow. Initially, even slight pressure differences across the bubble, induced by the external turbulent field, allow for gas movement within the relatively symmetrical deformed mother bubble. This movement is particularly facilitated by the low density and inertia of the gas phase. Consequently, one side of the bubble radius expands while the opposite side contracts, leading to an increasing pressure difference between the two sides. This increased internal flow is thus self-accelerating in its initial phase. In the later phase, the internal flow accelerates to such an extent that the resulting fluid dynamics create stress imbalance at the neck of the deformed bubble. Eventually,

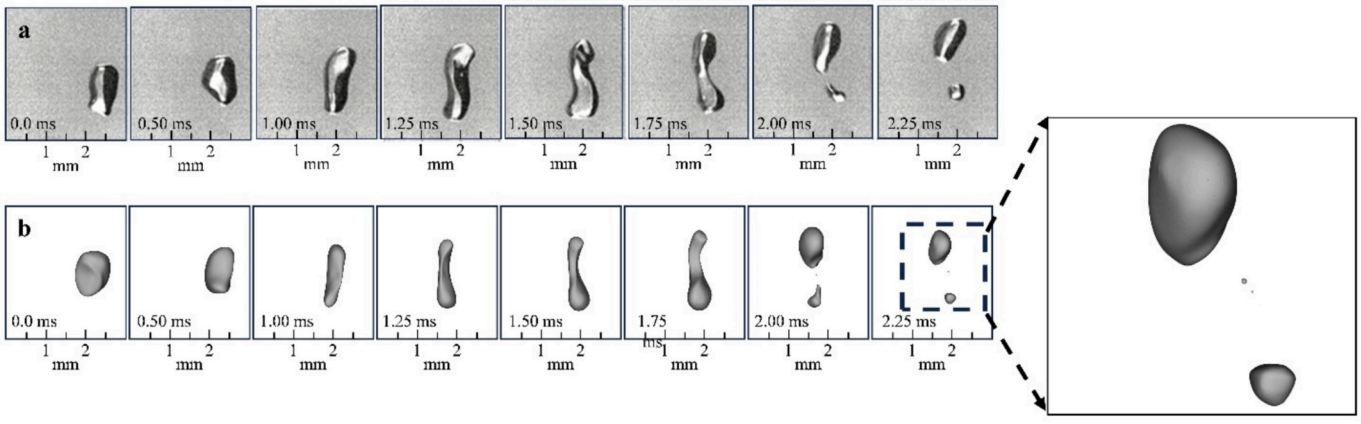

Fig. 5. Comparison between a) high-speed experimental measurement, b.) high-resolution simulation of the bubble breakup at We = 0.5.

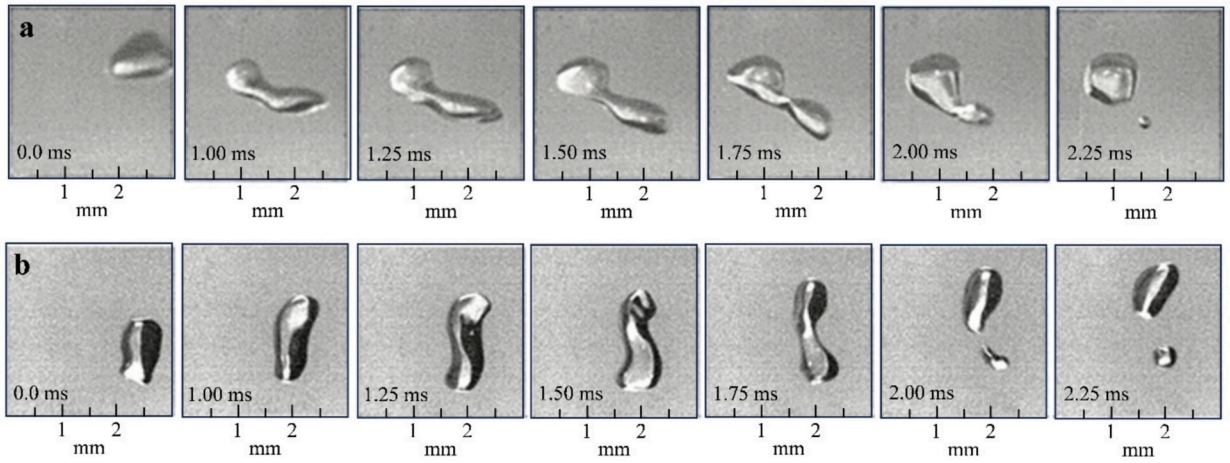

Fig. 6. Experimental measurements illustrating the stochastic behavior of the bubble breakup in turbulent flows, a) breakup volume fraction = 98 %, b) breakup volume fraction = 84 % at We = 0.5.

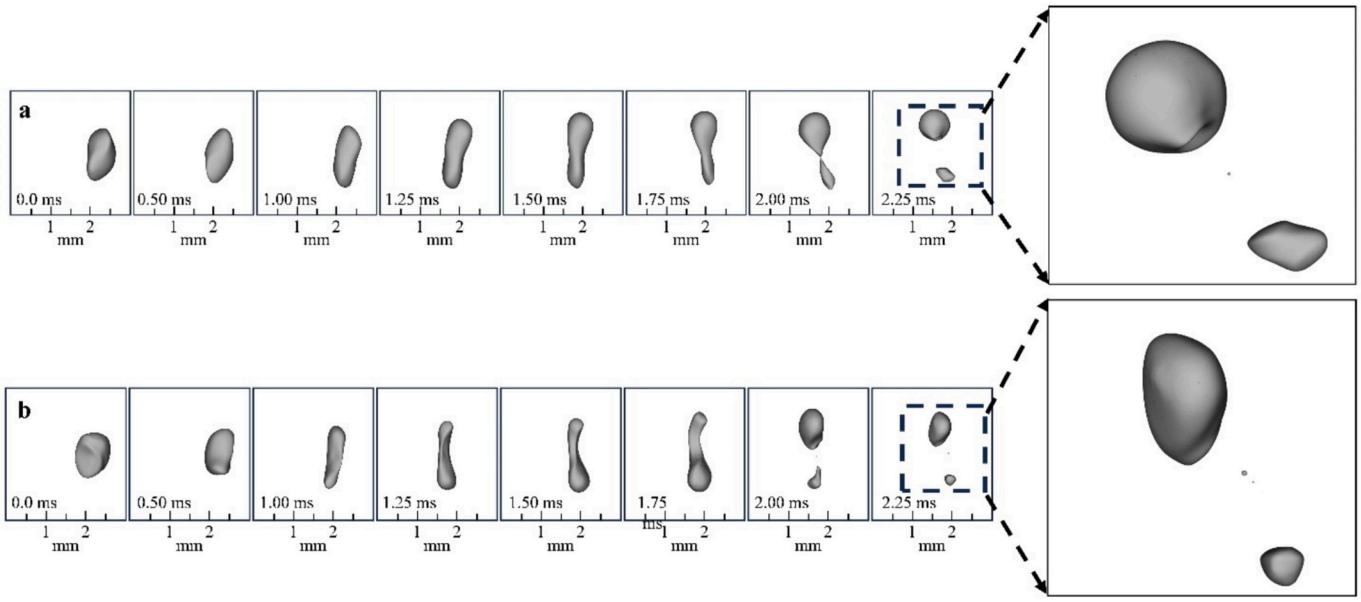

Fig. 7. Simulations showing the typical variation of the outcome from bubble breakup in turbulent flows at We = 0.5.

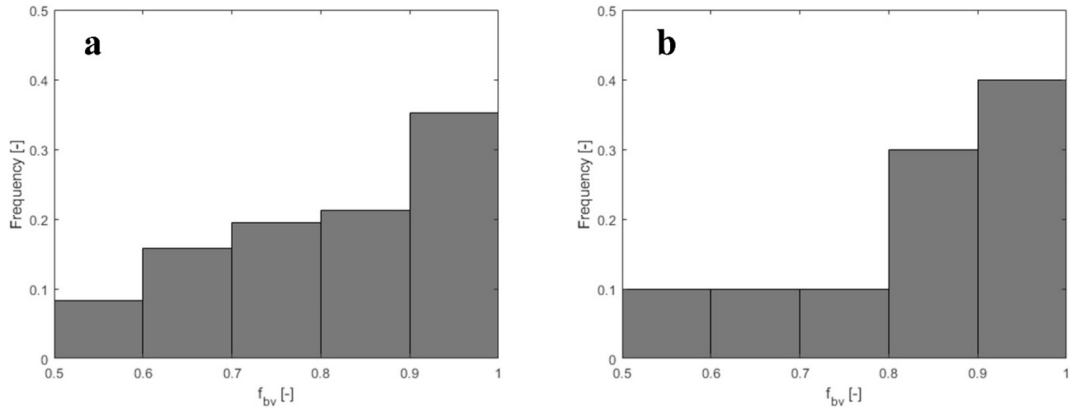

Fig. 8. Daughter size distribution for the range of We = 0.3 – 0.5, a.) experimental observations, and b.) simulation data.

this culminates in the collapse of the bubble neck before all the gas has been fully transferred.

Although various models predict bubble breakup fragmentation, validation is limited to high-speed imaging, lacking data on internal flow mechanisms like flow field, pressure distribution, and stress dynamics. Fig. 9 illustrates the sequence of increasing internal flow, with vectors indicating movement from the smaller end of the bubble to the larger end. For clarity, these vectors are scaled at different levels while maintaining the same color bar throughout the sequence in Fig. 9(a-d). Notably, the internal gas velocity rises rapidly from 0 m/s to 30 m/s in a fraction of a millisecond, and the flow through the neck stops at moment of neck rupture, ultimately leading to breakup into fragments of unequal sizes, due to the rapid redistribution of gas inside the bubble.

The corresponding velocity profiles across the bubble neck can be seen in Fig. 10. Although the flow is slightly asymmetrical, due to variation in flow fields on the different sides, a parabolic shape is evident, consistently showing a clear maximum velocity at the center of the neck at all times, which aligns with theoretical expectations.

Fig. 11 shows the development and increase of the internal static pressure, using a reference pressure on the larger side of the deformed bubble, which drives the development of an internal gas flow through the neck. By utilizing the reference pressure within the larger side of the deformed bubble, it becomes easier to compare the variations in internal pressure distribution over time. This is because the internal pressure differences are minor compared to the reactors operating pressure of 1 atmosphere. Initially, the pressure distribution is uniform. However, at a later stage, the static pressure becomes significantly higher in the smaller part of the deformed bubble. As the internal flow accelerates, the static pressure reaches a minimum at the neck, and the pressure difference across the neck continues to increase over time. The pressure distribution over the neck region exhibits similarities to those observed in nozzles and orifices, where a local minimum in static pressure typically occurs near the contraction due to the vena contracta effect. The neck region of the deformed bubble experiences similar effects, resulting in local negative pressure, which is in absolute terms positive and close to the reactors operating pressure. Additionally, changes in neck dimension as well as the accelerating flow over time, and existence of an interface rather than a rigid wall in the contraction region make the process more complex compared to hydrodynamics in classical static nozzles and orifices. This highlights the need for detailed simulations to study and understand the transient phenomena.

This pressure difference escalates within a fraction of a millisecond and rapidly shifting balance of stresses at the neck interface ultimately leads to the breakup of the bubble. Therefore, the internal flow mechanism is a rapid and complex process that necessitates extremely high temporal and spatial resolution for precise observation, which surpasses the capabilities of current experimental methods.

Experimental data indicates that bubble breakup occurs when the neck diameter is reduced to between 1/3 and 1/2 of the initial diameter [28,49]. This estimation, however, is crude due to the limitations imposed by the time resolution of the experimental system. High-resolution simulations, on the other hand, permit a detailed quantification of the continuous deformation sequence, including neck diameter and stresses, up to the final breakup. Fig. 12 presents a local stress analysis calculated based on the relative velocity and neck diameter, suggesting that breakup occurs when the stresses intersect. This intersection typically occurs when the bubble neck diameter is reduced to 1/10 of the mother bubble's initial diameter.

Deformation of the bubble is initiated when the external turbulent stress is significant compared to the stabilizing cohesive interfacial stress. However, during the later deformation phase where a neck is formed and continues to shrink, the interfacial stress at the neck favors contraction of the neck. As the internal flow accelerates, the dynamic pressure estimated from the instantaneous maximum velocity at the neck increases with time, as described by Eq. (11). However, the inward-directed interfacial tension stress at the neck, as described by Eq. (12), rises more rapidly due to its inverse relationship with the local curvature. This results in a dominant contracting stress at the neck, which disrupts the flow before all the fluid can reach the opposite side, resulting in unequal sized fragments.

$$\tau_1(t) = \frac{\rho u^2_{max,internal}(t)}{2} \tag{11}$$

$$\tau_2(t) = \frac{\sigma}{2R_{neck}(t)} \tag{12}$$

A significant contribution towards understanding bubble breakup was made by Xing et al. [30] who developed a zero-dimensional mathematical model for bubble breakup that accounted for internal flow. However, their assumptions led to an overestimation of breakup time and an underprediction of the bubble breakup rate. Their model predicted a breakup time of close to 25 ms, whereas experimental data indicated a breakup time of approximately one order of magnitude lower. This discrepancy underscores the importance of making reasonable assumptions to develop more accurate theoretical models. Subsequently, Zhang et al. [31] revised these assumptions. The improved breakup model, which included more accurate estimations of the critical neck diameter (half the radius of the smaller fragment) and considered the interfacial cohesive stress, yielded predictions closely matching the experimental data [28]. The present study reveals that the ratio of the neck radius, $R_{neck}(t)$, to the radius at the smaller end of the bubble, $R_1(t)$, varies over time and should not be considered fixed. Fig. 13 illustrates the temporal evolution of the neck diameter, highlighting an acceleration in time.

Assumption of a constant ratio leads to differences in predicted daughter size distribution as noted by Zhang et al. [31], who relaxed this condition and yet assumed a constant but lower ratio of 0.5 to improve model predictions. The continuous process is illustrated in Fig. 14, which compares the observations made in this study with different theoretical model assumptions. Notably, these rapid changes in neck diameter occur within a fraction of a millisecond, typically around 0.2 ms. This necessitates a high-speed imaging system with a temporal

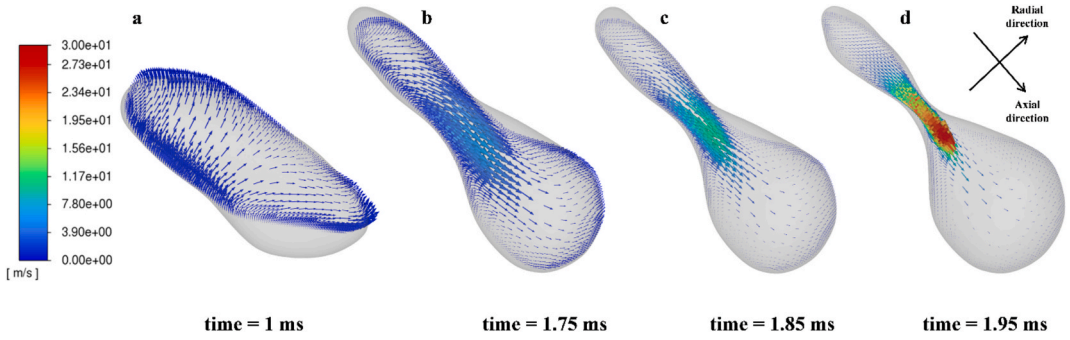

Fig. 9. Internal flow field within the gas bubble on a cross-sectional plane during the breakup process (vectors scaled for clarity), at a Weber number of 0.5.

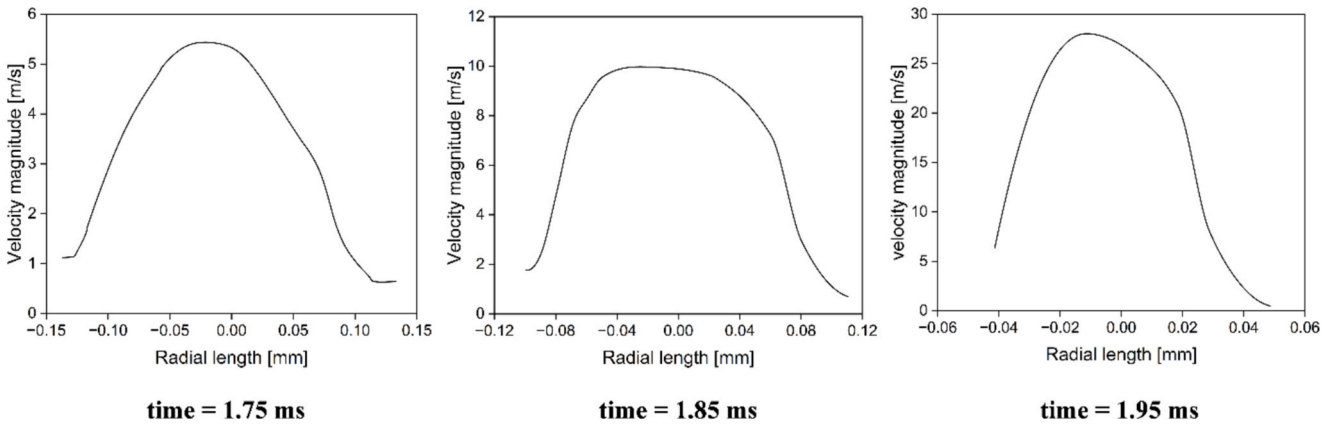

Fig. 10. Evolution of radial velocity profiles within the bubble neck prior to fragmentation at a Weber number of 0.5.

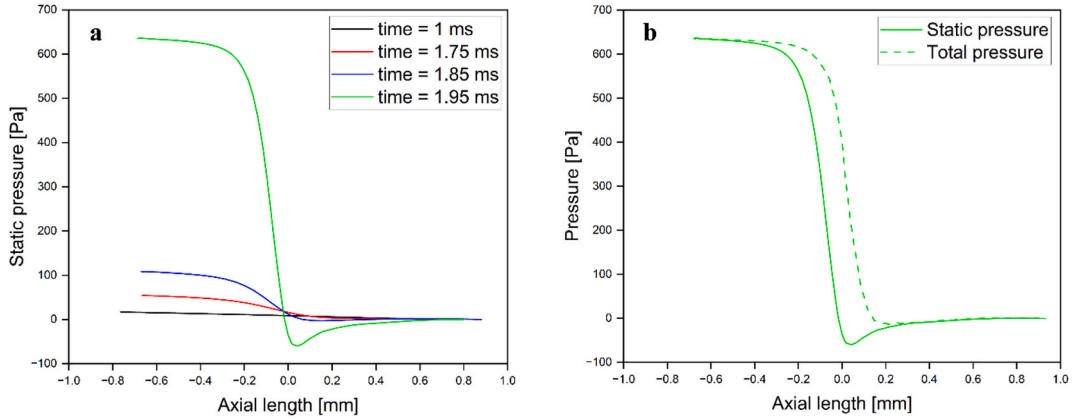

Fig. 11. a.) Evolution of the static pressure distribution along the axial direction within the deformed bubble during the breakup process, utilizing references pressure, at We = 0.5, b.) static and total pressure distribution at t = 1.95 ms.

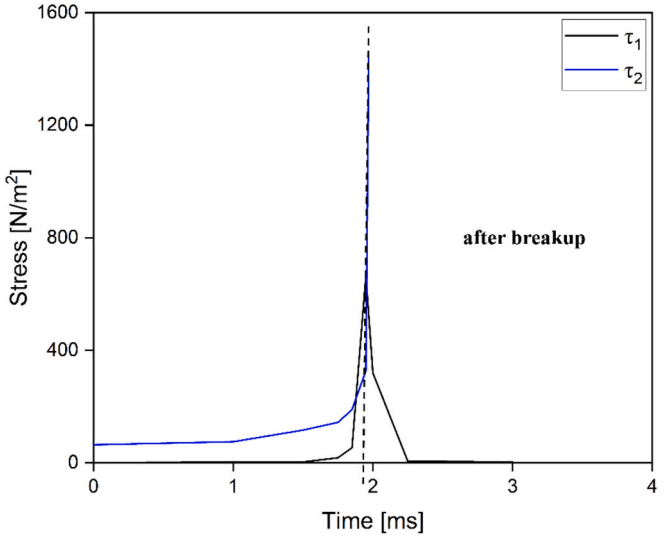

Fig. 12. Comparative analysis of stresses during bubble breakup at We = 0.5.

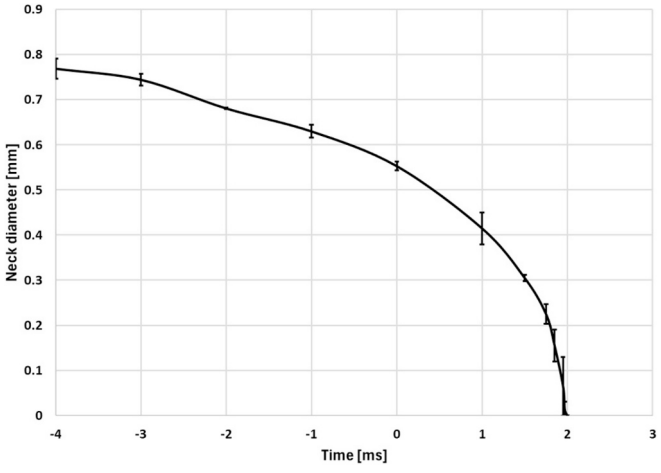

Fig. 13. Temporal variation of neck diameter until the final breakup of bubbles with internal flow at We = 0.5.

resolution of at least 20,000 fps to capture the redistribution flow effectively. Even at this frame rate, which is five times faster than the best currently reported visualization of single bubble breakup in the literature, only four images would be captured.

The larger error bars towards the end of the observed period may be attributed to the sensitivity of the neck, which experiences slight differences in external pressure across various cases. The results from this study show that detailed information on flow fields, pressure distribution, and bubble shapes during breakup enhances understanding of bubble dynamics. It is concluded that simulations offer superior temporal and spatial resolution, enable quantification of properties like internal bubble pressure fields and internal flow fields that experimental methods cannot measure. The data from this study allows for

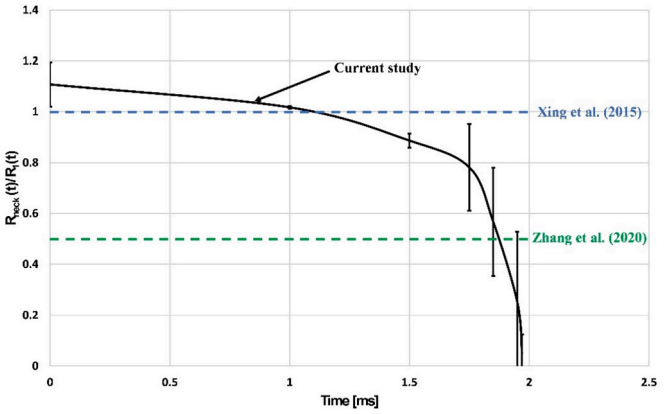

Fig. 14. Temporal evolution of the ratio $R_{neck}(t)/R_1(t)$ describing the dynamic deformation process leading up to bubble breakup.

verification and falsification of existing kernels. Enhancements of existing breakup kernels may relate to improving assumptions such as the dynamics of the ratio between the neck radius and the smaller fragment's radius during fragmentation in current kernels. More broadly, mechanistic explanations including insights into breakup time, dynamics of pressure distribution, unique quantification of the internal flow, and stresses, are invaluable for developing new kernels to accurately depict the stochastic nature of fragmentation.

5. Conclusions

The dynamics of bubble breakup under turbulent flow conditions were thoroughly investigated using experimental observations and development of high-resolution simulations. This approach revealed previously unattainable details of the dynamic process, by overcoming the limitations of temporal and spatial resolutions and the challenges posed by light reflection and refraction at gas–liquid interfaces. The three-dimensional transient simulations were successfully validated against experimental data obtained under identical hydrodynamic conditions, facilitating detailed analysis of properties that are otherwise unattainable through experimental methods alone. This included the quantification of three-dimensional interfacial dynamics, breakup time scales, and unique details on the internal flow mechanisms. Furthermore, quantifying the impact of vortex on bubble dynamics is regarded as a more advantageous approach compared to explicitly identifying the vortices. Current methodologies, such as the q-criterion and lambda-criterion, exhibit limitations as they primarily identify vortex cores without clearly defining their boundaries and they also depend on threshold criteria. The analysis revealed that the characteristic internal redistribution flow occurs within a fraction of a millisecond, necessitating a temporal resolution of at least 20,000 fps. An analysis of the internal flow mechanism during bubble breakup unveiled development of significant internal pressure gradients and flow velocities up to 30 times greater at the bubble neck compared to the mean bubble velocity. The development of an accelerating internal flow was quantified throughout the process until a sudden termination of the flow occurred due to the rapidly shifting balance of stresses at the interface. Experimental and simulation data showed that bubble breakup in turbulent conditions is random, leading to daughter fragments of different sizes that follow a U-shaped distribution. This pattern was consistently seen in both experiments and simulations. Evidence suggested that bubble breakup at higher Weber number can form satellite fragments like what is known from droplet breakup, but these are likely beyond the resolution capabilities of the most advanced experimental setups documented in single bubble breakup literature, which are constrained by imaging resolution and contrast limitations. Consequently, simulations offer superior temporal and spatial resolution and offer comprehensive understanding of bubble dynamics, surpassing current experimental capabilities. This simulation approach holds significant promises for improving future breakup rate models, thereby driving progress in the field and is anticipated to contribute to the development of refined breakup kernels. Although the simulations are currently very time-consuming, the expected leaps in computational capabilities will likely mitigate this challenge making high-resolution detailed studies more feasible and efficient.

CRediT authorship contribution statement

Vikash Vashisth: Writing – original draft, Visualization, Validation, Software, Methodology, Investigation, Formal analysis. **Ronnie Andersson:** Writing – review & editing, Supervision, Project administration, Investigation, Funding acquisition, Conceptualization.

Declaration of competing interest

The authors declare that they have no known competing financial interests or personal relationships that could have appeared to influence the work reported in this paper.

Acknowledgements

Financial support from the Swedish Research Council (Grant: 2020-05476) is gratefully acknowledged. The computations were enabled by resources provided by the National Academic Infrastructure for Supercomputing in Sweden (NAISS) at Chalmers e-Commons/C3SE and NSC Tetralith partially funded by the Swedish Research Council (Grant: 2022-06725).

Data availability

Data will be made available on request.

References

[1] A. Kolmogorov, On the breakage of drops in a turbulent flow, in: Dokl. Akad. Navk. SSSR, 1949: pp. 825–828.
[2] J.O. Hinze, Fundamentals of the hydrodynamic mechanism of splitting in dispersion processes, AIChE J. 1 (1955) 289–295.
[3] C.D. Eastwood, L. Armi, J.C. Lasheras, The breakup of immiscible fluids in turbulent flows, J. Fluid Mech. 502 (2004) 309–333, https://doi.org/10.1017/S0022112003007730.
[4] S. Maaß, A. Gäbler, A. Zaccone, A.R. Paschedag, M. Kraume, Experimental investigations and modelling of breakage phenomena in stirred liquid/liquid systems, Chem. Eng. Res. Des. 85 (2007) 703–709, https://doi.org/10.1205/cherd06187.
[5] J. Solsvik, H.A. Jakobsen, Single Air Bubble Breakup Experiments in Stirred Water Tank, Int. J. Chem. React. Eng. 13 (2015) 477–491, https://doi.org/10.1515/ijcre-2014-0154.
[6] J. Vejražka, M. Zedníková, P. Stanovský, Experiments on breakup of bubbles in a turbulent flow, AIChE J. 64 (2018) 740–757, https://doi.org/10.1002/aic.15935.
[7] F. Ravelet, C. Colin, F. Risso, On the dynamics and breakup of a bubble rising in a turbulent flow, Phys. Fluids 23 (2011), https://doi.org/10.1063/1.3648035.
[8] M. Ashar, D. Arlov, F. Carlsson, F. Innings, R. Andersson, Single droplet breakup in a rotor-stator mixer, Chem. Eng. Sci. 181 (2018) 186–198, https://doi.org/10.1016/j.ces.2018.02.021.
[9] E.H. Herø, N. La Forgia, J. Solsvik, H.A. Jakobsen, Single drop breakage in turbulent flow: Statistical data analysis, Chem. Eng. Sci. X 8 (2020), https://doi.org/10.1016/j.cesx.2020.100082.
[10] W. Shi, X. Yang, M. Sommerfeld, J. Yang, X. Cai, G. Li, Y. Zong, Modelling of mass transfer for gas-liquid two-phase flow in bubble column reactor with a bubble breakage model considering bubble-induced turbulence, Chem. Eng. J. 371 (2019) 470–485, https://doi.org/10.1016/j.cej.2019.04.047.
[11] J. Huang, L. Sun, M. Du, Z. Liang, Z. Mo, J. Tang, G. Xie, An investigation on the performance of a micro-scale Venturi bubble generator, Chem. Eng. J. 386 (2020) 120980, https://doi.org/10.1016/j.cej.2019.02.068.
[12] P. Moilanen, M. Laakkonen, O. Visuri, V. Alopaeus, J. Aittamaa, Modelling mass transfer in an aerated 0.2 m3 vessel agitated by Rushton, Phasejet and Combijet impellers, Chem. Eng. J. 142 (2008) 95–108, https://doi.org/10.1016/j.cej.2008.01.033.
[13] R. Ni, Annual Review of Fluid Mechanics Deformation and Breakup of Bubbles and Drops in Turbulence, Annu. Rev. (2024) 319–347, https://doi.org/10.1146/annurev-fluid-121021-.

[14] M. Petitti, M. Vanni, D.L. Marchisio, A. Buffo, F. Podenzani, Simulation of coalescence, break-up and mass transfer in a gas-liquid stirred tank with CQMOM, Chem. Eng. J. 228 (2013) 1182–1194, https://doi.org/10.1016/j.cej.2013.05.047.
[15] Q. Xiao, J. Wang, N. Yang, J. Li, Simulation of the multiphase flow in bubble columns with stability-constrained multi-fluid CFD models, Chem. Eng. J. 329 (2017) 88–99, https://doi.org/10.1016/j.cej.2017.06.008.
[16] E.K. Nauha, Z. Kálal, J.M. Ali, V. Alopaeus, Compartmental modeling of large stirred tank bioreactors with high gas volume fractions, Chem. Eng. J. 334 (2018) 2319–2334, https://doi.org/10.1016/j.cej.2017.11.182.
[17] K. Guo, T. Wang, Y. Liu, J. Wang, CFD-PBM simulations of a bubble column with different liquid properties, Chem. Eng. J. 329 (2017) 116–127, https://doi.org/10.1016/j.cej.2017.04.071.
[18] Y. Chen, J. Ding, P. Weng, X. Yang, W. Wu, On the breakup of Taylor length scale size bubbles and droplets in turbulent dispersions, Chem. Eng. J. 386 (2020) 121826, https://doi.org/10.1016/j.cej.2019.05.187.
[19] J.C. Lasheras, C. Eastwood, C. Martínez-Bazán, J.L. Montaes, A review of statistical models for the break-up an immiscible fluid immersed into a fully developed turbulent flow, Int. J. Multiph. Flow 28 (2002) 247–278, https://doi.org/10.1016/S0301-9322(01)00046-5.
[20] Y. Liao, D. Lucas, A literature review of theoretical models for drop and bubble breakup in turbulent dispersions, Chem. Eng. Sci. 64 (2009) 3389–3406, https://doi.org/10.1016/j.ces.2009.04.026.
[21] J. Solsvik, S. Tangen, H.A. Jakobsen, On the constitutive equations for fluid particle breakage, Rev. Chem. Eng. 29 (2013) 241–356, https://doi.org/10.1515/revce-2013-0009.
[22] H.K. Foroushan, H.A. Jakobsen, On the dynamics of fluid particle breakage induced by hydrodynamic instabilities: A review of modelling approaches, Chem. Eng. Sci. 219 (2020) 115575, https://doi.org/10.1016/j.ces.2020.115575.
[23] G. Narsimhan, J.P. Gupta, D. Ramkrishna, A model for transitional breakage probability of droplets in agitated lean liquid-liquid dispersions, Chem. Eng. Sci. 34 (1979) 257–265, https://doi.org/10.1016/0009-2509(79)87013-X.
[24] C. Tsouris, L.L. Tavlarides, Breakage and coalescence models for drops in turbulent dispersions, AIChE J. 40 (1994) 395–406, https://doi.org/10.1002/aic.690400303.
[25] H. Luo, H.F. Svendsen, Theoretical Model for Drop and Bubble Breakup in Turbulent Dispersions, AIChE J. 42 (1996) 1225–1233, https://doi.org/10.1002/aic.690420505.
[26] L. Hagesaether, H.A. Jakobsen, H.F. Svendsen, A model for turbulent binary breakup of dispersed fluid particles, Chem. Eng. Sci. 57 (2002) 3251–3267, https://doi.org/10.1016/S0009-2509(02)00197-5.
[27] T. Wang, J. Wang, Y. Jin, A novel theoretical breakup kernel function for bubbles/droplets in a turbulent flow, Chem. Eng. Sci. 58 (2003) 4629–4637, https://doi.org/10.1016/j.ces.2003.07.009.
[28] R. Andersson, B. Andersson, On the breakup of fluid particles in turbulent flows, AIChE J. 52 (2006) 2020–2030, https://doi.org/10.1002/aic.10831.
[29] R. Andersson, B. Andersson, Modeling the breakup of fluid particles in turbulent flows, AIChE J. 52 (2006) 2031–2038, https://doi.org/10.1002/aic.10832.
[30] C. Xing, T. Wang, K. Guo, J. Wang, A unified theoretical model for breakup of bubbles and droplets in turbulent flows, AIChE J. 61 (2015) 1391–1403, https://doi.org/10.1002/aic.14709.
[31] H. Zhang, G. Yang, A. Sayyar, T. Wang, An improved bubble breakup model in turbulent flow, Chem. Eng. J. 386 (2020) 121484, https://doi.org/10.1016/j.cej.2019.04.064.
[32] K. Razzaghi, F. Shahraki, Theoretical model for multiple breakup of fluid particles in turbulent flow field, AIChE J. 62 (2016) 4508–4525, https://doi.org/10.1002/aic.15314.
[33] R. Andersson, A. Helmi, Computational fluid dynamics simulation of fluid particle fragmentation in turbulent flows, Appl. Math. Model. 38 (2014) 4186–4196, https://doi.org/10.1016/j.apm.2014.01.005.
[34] M. Karimi, R. Andersson, Stochastic simulation of droplet breakup in turbulence, Chem. Eng. J. 380 (2020) 122502, https://doi.org/10.1016/j.cej.2019.122502.
[35] P. Liovic, D. Lakehal, Interface-turbulence interactions in large-scale bubbling processes, Int. J. Heat Fluid Flow 28 (2007) 127–144, https://doi.org/10.1016/j.ijheatfluidflow.2006.03.003.
[36] P.K. Farsoiya, Z. Liu, A. Daiss, R.O. Fox, L. Deike, Role of viscosity in turbulent drop break-up, J. Fluid Mech. 972 (2023) 1–17, https://doi.org/10.1017/jfm.2023.684.
[37] A. Håkansson, L. Brandt, Deformation and initial breakup morphology of viscous emulsion drops in isotropic homogeneous turbulence with relevance for emulsification devices, Chem. Eng. Sci. 253 (2022), https://doi.org/10.1016/j.ces.2022.117599.
[38] A. Håkansson, M. Crialesi-Esposito, L. Nilsson, L. Brandt, A criterion for when an emulsion drop undergoing turbulent deformation has reached a critically deformed state, Colloids Surfaces A Physicochem. Eng. Asp. 648 (2022) 129213, https://doi.org/10.1016/j.colsurfa.2022.129213.
[39] P. Olad, F. Innings, M. Crialesi-Esposito, L. Brandt, A. Håkansson, Comparison of turbulent drop breakup in an emulsification device and homogeneous isotropic turbulence: Insights from numerical experiments, Colloids Surfaces A Physicochem. Eng. Asp. 657 (2023) 130569, https://doi.org/10.1016/j.colsurfa.2022.130569.
[40] R. Andersson, B. Andersson, F. Chopard, T. Norén, Development of a multi-scale simulation method for design of novel multiphase reactors, Chem. Eng. Sci. 59 (2004) 4911–4917, https://doi.org/10.1016/j.ces.2004.07.084.
[41] S.B. Pope, Turbulent Flows, Meas. Sci. Technol. 12 (2001) 2020, https://doi.org/10.1088/0957-0233/12/11/705.
[42] Andersson B. Andersson R. Håkansson L. Mortensen M. Sudiyo R. Wachem B. Computational fluid dynamics for engineers 2011 Cambridge University Press Cambridge 10.1017/CBO9781139093590.
[43] D.K. Lilly, A proposed modification of the Germano subgrid-scale closure method, Phys. Fluids A 4 (1992) 633–635, https://doi.org/10.1063/1.858280.
[44] J.U. Brackbill, D.B. Kothe, C. Zemach, A continuum method for modeling surface tension, J. Comput. Phys. 100 (1992) 335–354, https://doi.org/10.1016/0021-9991(92)90240-Y.
[45] S.B. Pope, Ten questions concerning the large-eddy simulation of turbulent flows, New J. Phys. 6 (2004), https://doi.org/10.1088/1367-2630/6/1/035.
[46] C.A. Coulaloglou, L.L. Tavlarides, Description of interaction processes in agitated liquid-liquid dispersions, Chem. Eng. Sci. 32 (1977) 1289–1297, https://doi.org/10.1016/0009-2509(77)85023-9.
[47] M. Konno, Y. Matsunaga, K. Arai, S. Saito, Simulation model for breakup process in an agitated tank, J. Chem. Eng. Japan 13 (1980) 67–73, https://doi.org/10.1252/jcej.13.67.
[48] S. Maaß, M. Kraume, Determination of breakage rates using single drop experiments, Chem. Eng. Sci. 70 (2012) 146–164, https://doi.org/10.1016/j.ces.2011.08.027.
[49] B.O. Hasan, Experimental study on the bubble breakage in a stirred tank. Part 1. Mechanism and effect of operating parameters, Int. J. Multiph. Flow 97 (2017) 94–108, https://doi.org/10.1016/j.ijmultiphaseflow.2017.08.006.